Forward–Backward Method for Scattering from Imperfect Conductors

Dennis Holliday, Lester L. DeRaad, Jr., and Gaetan J. St-Cyr

***Abstract*— The previously developed forward–backward method for calculating scattering from perfectly conducting azimuthally homogeneous surfaces is extended to imperfect conductors, where the dielectric constant has a large imaginary part such as sea water at X-band (10 GHz). An example shows that highly accurate results at X-band are obtained for the case of a steepened sea wave.**

***Index Terms*—Sea surface electromagnetic scattering.**

I. Introduction

In a previous paper [1], we proposed a new method called forward–backward for solving the magnetic field integral equation (MFIE) for a perfectly conducting azimuthally homogeneous surface under conditions where there is significant low-grazing angle backscatter. We now describe the extension of the new method to scattering from imperfect conductors with dielectric constants near that of sea water, i.e., $\epsilon = 65 + i40$ at 3-cm incident radiation [2].

II. Derivation of Equations

We consider an azimuthally homogeneous surface S that divides space into two regions. The vertical and horizontal coordinates of this surface, $z(\ell)$ and $y(\ell)$, respectively, are functions of the path length ℓ on the surface; for $\ell > \ell_+$ and $\ell < \ell_-$, $z = 0$, i.e., the surface is flat outside a specified region. Region 1 is a vacuum, which has a dielectric constant ϵ of one and permeability μ of one and contains $z \Rightarrow +\infty$. The sources of electromagnetic radiation that impinge on S are all located in Region 1. Region 2 contains $z \Rightarrow -\infty$ and is a nonmagnetic $(\mu = 1)$ material media characterized by a complex dielectric constant ϵ.

For brevity, we first consider the scattering of an H-pol incident plane wave of unit amplitude; the equations describing the scattering of a V-pol incident plane wave of unit amplitude will be derived from the H-pol equation by well-known substitution rules [3].

To apply the forward–backward method to scattering from imperfect conductors, we will find it convenient to write the well-known equations relating the electric current $L_H(\ell) = \hat{t}(\ell) \cdot [\hat{n}(\ell) \times \mathbf{E}]$ and magnetic current $J_H(\ell) = \hat{x} \cdot [\hat{n}(\ell) \times \mathbf{B}]$ on S in the form [3]

$$L_H(\ell) = 2e^{-i\phi(\ell)} + \frac{i}{2}\kappa \int_{-\infty}^{+\infty} d\ell' \{L_H(\ell')\hat{n}(\ell')\hat{\gamma} H_1^{(1)}(\kappa\gamma) + iJ_H(\ell')H_0^{(1)}(\kappa\gamma)\} \tag{1}$$

$$L_H(\ell) = -\frac{i}{2}\kappa \int_{-\infty}^{+\infty} d\ell' \Big\{ L_H(\ell')\sqrt{\epsilon}\hat{n}(\ell') \cdot \hat{\gamma} H_1^{(1)}(Z) + iJ_H(\ell')H_0^{(1)}(Z) \Big\} \tag{2}$$

where the vector $\boldsymbol{\gamma}$ is $\boldsymbol{\gamma}(\ell, \ell') = [y(\ell) - y(\ell'),\ z(\ell) - z(\ell')]$ and $Z = \sqrt{\epsilon}\kappa|\boldsymbol{\gamma}|$; the unit normal vector and unit tangent vector to S are given by $\hat{n}(\ell) = [-z'(\ell), y'(\ell)]$ and $\hat{t}(\ell) = [y'(\ell), z'(\ell)]$, respectively; $\hat{x}$ is the unit vector in the azimuthal direction. The phase of the incident plane wave is $\phi(\ell) = \kappa[\sin\theta y(\ell) + \cos\theta z(\ell)]$, where κ is its wavenumber and θ is its incidence angle. The functions $H_n^{(1)}$ are Hankel functions of the first kind of order n.

Equations (1) and (2) can be put in a form that facilitates their numerical solution. Define

$$L_H(\ell) = L_0 e^{-i\phi(\ell)} + L_{HR}(\ell) \tag{3}$$

where

$$L_0 = 2\cos\theta \Big/ \Big[\cos\theta + \sqrt{\epsilon - \sin^2\theta}\Big]. \tag{4}$$

A function $J_{H0}(\ell)$ is obtained by inverting

$$L_0 e^{-i\phi(\ell)} = -\frac{i}{2}\kappa \int_{-\infty}^{+\infty} d\ell' \Big\{ L_0 e^{-i\phi(\ell')}\sqrt{\epsilon}\hat{n}(\ell') \cdot \hat{\gamma} H_1^{(1)}(Z) + iJ_{H0}(\ell')H_0^{(1)}(Z) \Big\} \tag{5}$$

by a standard method, which will be discussed in Appendix A. Next, we define $J_{HR}(\ell)$ by

$$J_H(\ell) = J_{H0}(\ell) + J_{HR}(\ell) \tag{6}$$

which leads to the following equations satisfied by $L_{HR}(\ell)$ and $J_{HR}(\ell)$:

$$L_{HR}(\ell) = D_H(\ell) + \frac{i}{2}\kappa \int_{-\infty}^{+\infty} d\ell' \{L_{HR}(\ell')\hat{n}(\ell') \cdot \hat{\gamma} H_1^{(1)}(\kappa\gamma) + iJ_{HR}(\ell')H_0^{(1)}(\kappa\gamma)\} \tag{7}$$

Manuscript received September 11, 1996; revised August 18, 1997. This work was supported by the Department of Defense Contract DMA800-94-C-6010.

The authors are with Logicon, Los Angeles, CA 90009 USA.

Publisher Item Identifier S 0018-926X(98)01038-2.

TABLE I
H-POL TO V-POL REPLACEMENTS

$L_H(\ell) \Rightarrow J_V(\ell)$	
where $J_V(\ell) = \hat{t}(\ell) \cdot [\hat{n}(\ell) \times \mathbf{B}]$	
$J_H(\ell) \Rightarrow -\begin{bmatrix} 1 \\ \epsilon \end{bmatrix} L_V(\ell)$	use the ϵ in Eq. (2)
where $L_V(\ell) = \hat{x} \cdot [\hat{n}(\ell) \times \mathbf{E}]$	
$L_0 \Rightarrow J_0$	see next entry
$\sqrt{\epsilon - \sin^2\theta} \Rightarrow \frac{1}{\epsilon}\sqrt{\epsilon - \sin^2\theta}$	
$L_{HR} \Rightarrow J_{VR}$	
$J_{H0} \Rightarrow -\begin{bmatrix} 1 \\ \epsilon \end{bmatrix} L_{V0}$	use the ϵ in Eq. (5)
$J_{HR} \Rightarrow -\begin{bmatrix} 1 \\ \epsilon \end{bmatrix} L_{VR}$	use the ϵ in Eq. (8)
$D_H \Rightarrow D_V$	with other changes noted above
$\mathbf{E}_S \Rightarrow \mathbf{B}_S$	
$\mathcal{B}_H \Rightarrow -\mathcal{B}_V$	with other changes noted above

and

$$L_{HR}(\ell) = -\frac{i}{2}\kappa \int_{-\infty}^{+\infty} d\ell' \Big\{ L_{HR}(\ell')\sqrt{\epsilon}\hat{n}(\ell')\hat{\gamma} H_1^{(1)}(Z) + iJ_{HR}(\ell')H_0^{(1)}(Z) \Big\} \tag{8}$$

where

$$D_H(\ell) = +\frac{i}{2}\kappa \int_{-\infty}^{+\infty} d\ell' \{2(L_0 - 1)e^{-i\phi(\ell')}\hat{n}(\ell') \cdot \hat{\gamma} H_1^{(1)}(\kappa\gamma) + i[J_{H0}(\ell') - (2 - L_0)e^{-i\phi(\ell')}\hat{n}(\ell')\hat{\kappa}]H_0^{(1)}(\kappa\gamma)\}. \tag{9}$$

The "transparency theorem" of Shaw and Dougan [4] has been used in the above derivation.

At large distances r from S, the azimuthal component of the scattered H-pol electric field is related to the surface currents by the Stratton–Chu equation [3]

$$\hat{x} \cdot \mathbf{E}_S(\hat{k}) \Rightarrow \frac{i}{2} \frac{e^{i(kr+\pi/4)}}{\sqrt{2\pi\kappa r}} \mathcal{B}_H(\hat{k}) \tag{10}$$

where

$$\mathcal{B}_H(\hat{k}) = \kappa \int_{-\infty}^{+\infty} \Big\{ [J_H(\ell') - \hat{n}(\ell') \cdot \hat{k} L_H(\ell')] \cdot e^{-i\kappa[y(\ell')\sin\theta_R + z(\ell')\cos\theta_R]} - \Big[\sqrt{\epsilon - \sin^2\theta} - \cos\theta_R\Big] L_0 y'(\ell') \cdot e^{-i\kappa[\sin\theta + \sin\theta_R]y(\ell')} \Big\} d\ell' \tag{11}$$

$$\hat{k} = (\sin\theta_R, \cos\theta_R) \tag{12}$$

θ_R being the angle of reflection so that for backscatter $\theta_R = \theta$; note that the component of the scattered field due to reflection of the incident wave from the plane $z = 0$ is subtracted so that $\mathcal{B}_H(\hat{k})$ represents that part of the scattering amplitude that varies as $1/\sqrt{r}$.

The above equations apply to the case where both the surface *and* the incident field is independent of the azimuthal coordinate. In nature, the part of the surface responsible for the azymptotic component of the scattered field, i.e., the part that varies as $1/\sqrt{r}$ will have a limited azimuthal extent ℓ_x. Provided that $\kappa\ell_x$ is large, the H-pol scattering cross section will be given by

$$\sigma_{HH} \cong \frac{\ell_x^2}{4\pi} |\mathcal{B}_H(\hat{k})|^2 \tag{13}$$

where $\mathcal{B}_H(\hat{k})$ is determined from (11). This approximation produces, for example, the ℓ_x^2 dependence of backscatter cross section from a straight edge [5].

For V-pol, the equations have the same structure and can be written down using the replacements indicated in Table I.

III. METHOD OF SOLUTION

The methods used to compute solutions to the above H-pol and V-pol Fredholm integral equations involve the conversion of each of the top-side equations [e.g., (7)] into two coupled Volterra equations, which are then solved by stepping. We have previously developed this method for scattering from perfect conductors and have named it forward–backward [1], which, for brevity, will be referred to as F/B. The bottom-side equations [e.g., (8) and its V-pol counterpart] will be solved by a method that involves approximating the Hankel function integrals. We will show the development only for H-pol and then use the substitution procedure in Table I to write the final V-pol equations.

Since $2\pi \cdot \mathrm{Im}\sqrt{\epsilon}$ is large ($\sim$12), the Hankel functions $H_0^{(1)}(Z)$ and $H_1^{(1)}(Z)$ are small except when ℓ' is within a

fraction of an electromagnetic wavelength of ℓ. Accordingly, we approximate the integral on the right-hand side of (8) by

$$-\frac{i}{2}\kappa \int_{-\infty}^{+\infty} d\ell' \Big\{ L_{HR}(\ell')\sqrt{\epsilon}\hat{n}(\ell')\cdot\hat{\gamma}H_1^{(1)}(Z) + iJ_{HR}(\ell')H_0^{(1)}(Z)\Big\} = A(\ell)L_{HR}(\ell) + D(\ell)J_{HR}(\ell) \tag{14}$$

where

$$A(\ell) = -\frac{i}{2}\kappa\sqrt{\epsilon}\int_{-\infty}^{+\infty} \hat{n}(\ell')\cdot\hat{\gamma}H_1^{(1)}(Z)\,d\ell' \tag{15}$$

and

$$D(\ell) = \tfrac{1}{2}\kappa \int_{-\infty}^{+\infty} H_0^{(1)}(Z)\,d\ell' \tag{16}$$

for a flat surface $A(\ell) = 0$ and $D(\ell) = (\epsilon)^{-(1/2)}$.

The above approximation in (14) is more accurate than a previously published "impedance boundary condition" approximation [6], which further approximates the integrals in (15) and (16) by taking

$$A(\ell) = -\frac{i}{2\kappa\sqrt{\epsilon}}\left[y'(\ell)z''(\ell) - z'(\ell)y''(\ell)\right] \tag{17}$$

$$D(\ell) = \frac{1}{\sqrt{\epsilon}}. \tag{18}$$

The accuracy of the approximations in (14) is discussed in Section V where it is shown to be good.

The values of $J_{HR}(\ell)$ and $L_{HR}(\ell)$ will be negligible far from the crests of the waves we will consider and a good approximation to (7) will be obtained by integrating ℓ' only over the interval $\ell_- \le \ell' \le \ell_+$, where ℓ_- and ℓ_+ are taken to be sufficiently far from the crest. Then, using the result

$$J_{HR}(\ell) = f_H(\ell)L_{HR}(\ell) \tag{19}$$

where

$$f_H(\ell) = \frac{1 - A(\ell)}{D(\ell)} \tag{20}$$

which is implied by (8) and (14), we obtain

$$L_{HR}(\ell) = D_H(\ell) + \int_{\ell_-}^{\ell_+} H(\ell,\,\ell')L_{HR}(\ell')\,d\ell' \tag{21}$$

where

$$H(\ell,\,\ell') = \frac{i}{2}\kappa\hat{n}(\ell')\cdot\hat{\gamma}H_1^{(1)}(\kappa\gamma) - \frac{\kappa}{2}f_H(\ell')H_0^{(1)}(\kappa\gamma). \tag{22}$$

The V-pol equations follow in exactly the same manner as the H-pol equations. We find

$$J_{VR}(\ell) = D_V(\ell) + \int_{\ell_-}^{\ell_+} V(\ell,\,\ell')J_{VR}(\ell')\,d\ell' \tag{23}$$

where

$$L_{VR} = -f_V(\ell)J_{VR}(\ell) \tag{24}$$

with

$$f_V(\ell) = f_H(\ell)/\epsilon \tag{25}$$

and

$$V(\ell,\,\ell') = \frac{i}{2}\kappa\hat{n}(\ell')\cdot\hat{\gamma}H_1^{(1)}(\kappa\gamma) - \frac{\kappa}{2}f_V(\ell')H_0^{(1)}(\kappa\gamma). \tag{26}$$

Equations (21) and (23) are solved by F/B. For (21) we write

$$L_{HR}(\ell) = L_{HR}^F(\ell) + L_{HR}^B(\ell) \tag{27}$$

where

$$L_{HR}^F(\ell) = D_H(\ell) + \int_{\ell}^{\ell_+} H(\ell,\,\ell')L_{HR}^B(\ell')\,d\ell' + \int_{\ell}^{\ell_+} H(\ell,\,\ell')L_{HR}^F(\ell')\,d\ell' \tag{28}$$

$$L_{HR}^B(\ell') = \int_{\ell_-}^{\ell} H(\ell,\,\ell')L_{HR}^F(\ell')\,d\ell' + \int_{\ell_-}^{\ell} H(\ell,\,\ell')L_{HR}^B(\ell')\,d\ell'. \tag{29}$$

Application of the F/B method begins with solving (28) with $L_{HR}^B = 0$ for L_{HR}^F by stepping starting at $\ell = \ell_+$ and proceeding to smaller ℓ. With the approximate L_{HR}^F so obtained we solve (29) for L_{HR}^B by stepping, starting at $\ell = \ell_-$ and proceeding to large ℓ. The resulting L_{HR}^B is then substituted into (28), which is then stepped to produce a new approximate L_{HR}^F. The procedure is continued until a desired degree of convergence is obtained. For this report we stopped the iterative process when the difference between successive estimates of L_{HR} is less than 10^{-4} at every point on the grid. Application of the F/B method to solve (23) proceeds in a similar manner that is straightforward to derive.

Some details of the computations are discussed in the Appendix. The accuracy of the method used in this section to obtain L_{HR}, J_{HR}, J_{VR}, and L_{VR} are discussed in Section V.

IV. Example: Backscatter from a Simulated Sea Wave

The preceding formulation has been used to compute L_H, J_H, J_V, L_V, and the H-pol and V-pol backscatter cross sections at 85° incidence angle (5° grazing) for a 10-GHz (3-cm wavelength) plane electromagnetic wave scattered from a simulated sea wave that is similar to a paddle-generated wave under investigation in the large wave tank at the Ocean Engineering Laboratory, University of California, Santa Barbara (UCSB). This simulated sea wave, which is in the deformation phase of breaking where the forward face has just moved past perpendicularity, is an output (Case 2.5, $t/T = 58.4377$, $T = 0.801$ s) of the LONGTANK numerical wavetank developed by Wang *et al.* at UCSB for the study of wave groups, wave–wave interactions, wave deformation, wave breaking, and other nonlinear effects [7]. Surface tension effects are taken into account in the computation of the wave shape. As shown in Fig. 1 (to scale), the wave, hereinafter called the UCSB wave, has a crest-to-trough amplitude of about 8 cm and its wavelength is about 1 m. Fig. 2 shows the detail of the forward face of the wave.

The wave shape data provided to us by Wang *et al.* in digital form comprises the whole wave group, which includes the

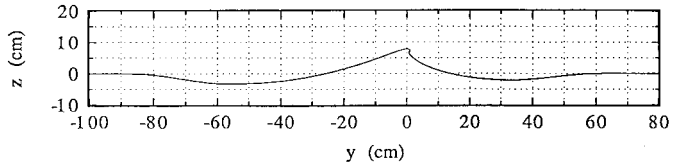

Fig. 1. UCSB wave.

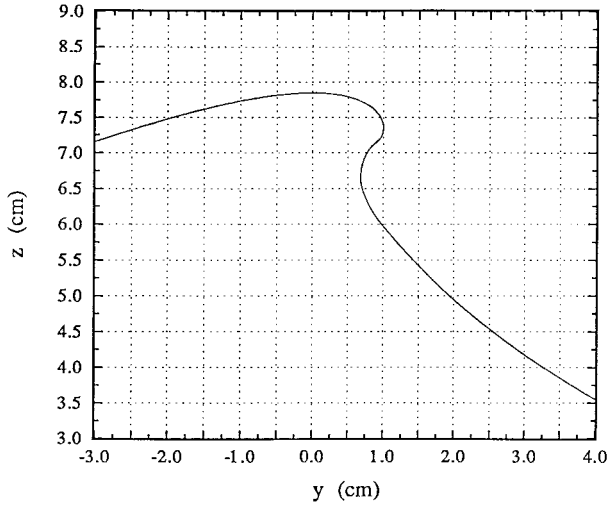

Fig. 2. Detail of the crest.

UCSB wave. For our example, we isolate the UCSB wave numerically by applying two "cosine-on-a-pedestal" functions to the whole group in such a way that the surface ahead of and behind the crest of the UCSB wave is brought smoothly to the mean ($z = 0$) water level as shown in Fig. 1.

Fig. 3 shows the computed values of $|L_H|$ and $|J_H|$ from $\ell = -10 + 10$ cm, while Fig. 4 shows the values of $|J_V|$ and $|L_V|$ over the same range; the perfectly conducting ($\epsilon \Rightarrow i\infty$) currents $|J_{HC}|$ and $|J_{VC}|$—computed by F/B—are also shown. The $|L_H|$ and $|L_V|$ are, as expected from (20) and (24), attenuated versions of $|J_H|$ and $|J_V|$. $|J_H|$ and $|J_{HC}|$ are similar, which is a consequence of negligible absorption in H-pol by the sea water. However, in V-pol, there is significant absorption at the low-grazing angle of our example, so $|J_V|$ and $|J_{VC}|$ are quite different. The backscatter amplitudes calculated from (11) and the corresponding V-pol expression with the above currents are

$$\mathcal{B}_H(\hat{\kappa}) = 27.1 \exp(-i\,23.1^\circ) \tag{30}$$

and

$$\mathcal{B}_V(\hat{\kappa}) = 3.2 \exp(-i\,11.5^\circ) \tag{31}$$

which, for a reference width of $\ell_x = 1$ m, leads to backscatter cross sections

$$\sigma_{HH} = 58.3 \text{ m}^2 \qquad (\sigma^C_{HH} = 98.2 \text{ m}^2) \tag{32}$$

and

$$\sigma_{VV} = 0.82 \text{ m}^2 \qquad (\sigma^C_{VV} = 24.3 \text{ m}^2) \tag{33}$$

the values in parentheses are those for perfect conductivity. The above value of σ_{HH} is in the range observed for large sea spikes [8]. As expected, σ_{HH} differs very little from σ^C_{HH}.

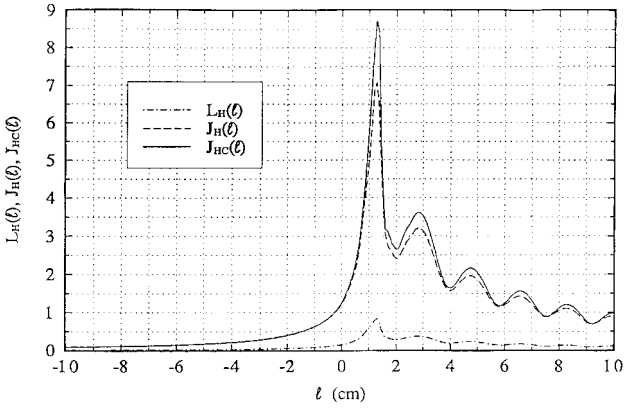

Fig. 3. H-pol currents.

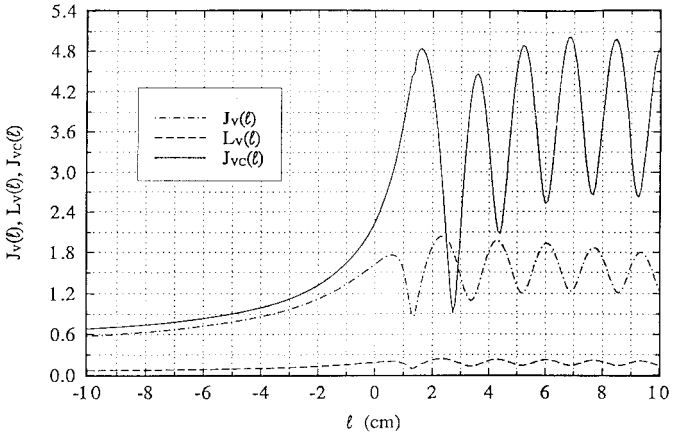

Fig. 4. V-pol currents.

However, due to the differences in backscatter produced by the effects of imperfect conductivity (which are complicated!), σ_{VV} differs from σ^C_{VV} by a much larger amount, 15 dB. The ratio of σ_{HH} to σ_{VV} is +19 dB, while the ratio of σ^C_{HH} to σ^C_{VV} is +6 dB.

To see the importance of multiple scattering in this example, we note that the Kirchhoff approximation to perfect conductivity backscatter from the UCSB wave leads to

$$\sigma^C_{\text{Kirch}} = 2.9 \text{ m}^2. \tag{34}$$

This value is 15 dB below σ^C_{HH} and 9 dB below σ^C_{VV}, thus showing that multiple scattering effects are significant in both H-pol and V-pol.

We have not been able to devise a "simple" explanation of the scattering phenomena that lead to the results computed above. Complicated interference phenomena, absorption by the sea water in V-pol, and scattering by highly curved regions of the surface are all involved in a significant way. What we have done is to develop a method to compute scattering from imperfectly conducting wave-like surfaces to a high degree of accuracy that can be verified.

V. Errors and Their Reaction

The simplest error check is to calculate how well the F/B solutions $L^F_{HR} + L^B_{HR}$ and $J^F_{VR} + J^B_{VR}$ satisfy the original

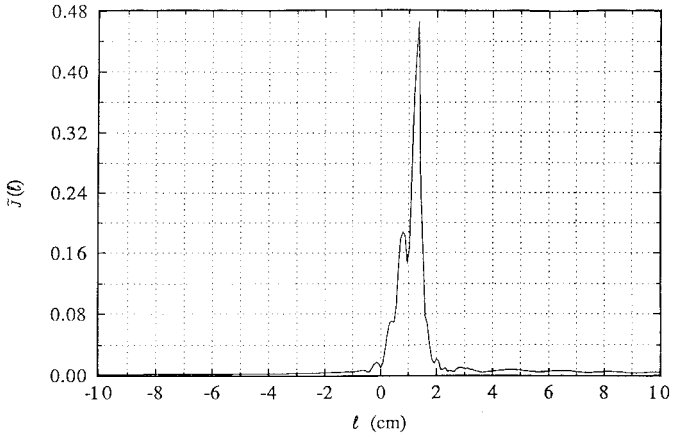

Fig. 5. $\tilde{J}$ for H-pol.

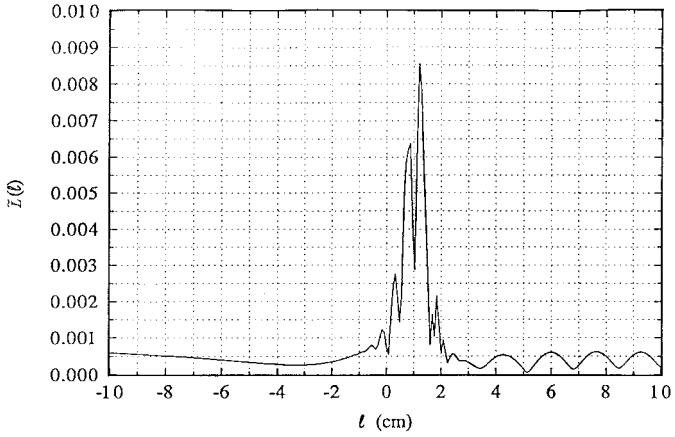

Fig. 6. $\tilde{L}$ for V-pol.

integral equations for L_{HR} and J_{VR} [(21), (23)], respectively. Direct substitution of the F/B solutions into the appropriate equations yield estimates of the errors. The maximum L_{HR} error occurs in the vicinity of the peak L_{HR} and is about 4 $\times$ 10^{-3}. The maximum error for J_{VR} is also located in the peak J_{VR} region and is very small at about 3 $\times$ 10^{-6}. If these errors are included in the calculation of the backscatter, they lead to negligible changes of 0.01 and 0.00 dB in the backscatter cross sections for H-pol and V-pol, respectively.

The above errors, of course, do not address the adequacy of the f_H and f_V approximations. We can consider these errors by introducing residual fields $\tilde{J}(\ell)$ and $\tilde{L}(\ell)$ as

$$\begin{aligned} J_{HR}(\ell) &= f_H(\ell) L_{HR}(\ell) + \tilde{J}(\ell) \\ L_{VR}(\ell) &= -f_V(\ell) J_{VR}(\ell) + \tilde{L}(\ell). \end{aligned} \tag{35}$$

The bottom-side integral equations for these residuals are

$$\begin{aligned} &\tfrac{1}{2}\kappa \int_{-\infty}^{\infty} d\ell' \tilde{J}(\ell') H_0^{(1)}(Z) \\ &\quad = L_{HR}(\ell) + \frac{i}{2}\kappa\sqrt{\epsilon} \int_{-\infty}^{+\infty} d\ell' L_{HR}(\ell') \hat{n}(\ell') \cdot \hat{\gamma} H_1^{(1)}(Z) \\ &\qquad - \tfrac{1}{2}\kappa \int_{-\infty}^{+\infty} d\ell' f_H(\ell') L_{HR}(\ell') H_0^{(1)}(Z) \end{aligned} \tag{36}$$

and

$$\begin{aligned} &\tfrac{1}{2}\kappa \int_{-\infty}^{\infty} d\ell' \tilde{L}(\ell') H_0^{(1)}(Z) \\ &\quad = -\left[J_{VR}(\ell) + \frac{i}{2}\kappa\sqrt{\epsilon} \int_{-\infty}^{+\infty} d\ell' J_{VR}(\ell') \hat{n}(\ell') \hat{\gamma} H_1^{(1)}(Z) \right] \Big/ \epsilon \\ &\qquad + \tfrac{1}{2}\kappa \int_{-\infty}^{+\infty} d\ell' f_V(\ell') J_{VR}(\ell') H_0^{(1)}(Z). \end{aligned} \tag{37}$$

Solutions for $\tilde{J}$ and $\tilde{L}$ are obtained in exactly the same way as the solution for $J_{H0}(\ell)$ and $L_{V0}(\ell)$ (see Appendix). Figs. 5 and 6 show the absolute values of $\tilde{J}$ and $\tilde{L}$, respectively, in the peak region, -10 cm $\leq \ell \leq$ 10 cm. As can be seen, these quantities are small compared to J_H and L_V and are concentrated in the region of the waveform that we expect to have the greatest error associated with f_H and f_V. When the residual currents $\tilde{J}$ and $\tilde{L}$ are used to calculate backscatter, the changed cross sections are again negligible: -0.02 and -0.05 dB for H-pol and V-pol, respectively.

The above discussion indicates that the original F/B solutions are highly accurate and yield highly accurate backscatter cross sections. However, the residuals can also be used for a procedure to determine more accurate solutions. In particular, if J_{HR} and L_{VR} are defined as in (35), then the appropriate integral equations for L_{HR} and J_{VR} [cf. (21), (23)] are

$$\begin{aligned} L_{HR}(\ell) = D_H(\ell) &- \tfrac{1}{2}\kappa \int_{-\infty}^{+\infty} d\ell' \tilde{J}(\ell') H_0^{(1)}(\kappa\gamma) \\ &+ \int_{-\infty}^{+\infty} d\ell' H(\ell, \ell') L_{HR}(\ell') \end{aligned} \tag{38}$$

and

$$\begin{aligned} J_{VR}(\ell) = D_V(\ell) &+ \tfrac{1}{2}\kappa \int_{-\infty}^{+\infty} d\ell' \tilde{L}(\ell') H_0^{(1)}(\kappa\gamma) \\ &+ \int_{-\infty}^{+\infty} d\ell' V(\ell, \ell') J_{VR}(\ell'). \end{aligned} \tag{39}$$

When combined with (36) and (37), the above equations comprise a complete set that can be solved iteratively. The iteration scheme starts with $\tilde{J} = \tilde{L} = 0$; (38) and (39) are solved for L_{HR} and J_{VR} by F/B. These solutions are then used to calculate $\tilde{J}$ and $\tilde{L}$ by means of (36) and (37). The new $\tilde{J}$ and $\tilde{L}$ are used in (38) and (39), which are then solved by F/B for a new L_{HR} and a new J_{VR}. We then go back to (36) and (37) and repeat the process. We stop the process when a criterion is met such as successive changes in $\tilde{J}$ and $\tilde{L}$ being less than some small number.

The iterative process described above was carried out for the surface under consideration. Table II lists the maximum changes in $\tilde{J}$ and $\tilde{L}$ as a function of iteration number starting with zero (the $\tilde{J} = \tilde{L} = 0$ solution discussed above). As can be seen, the procedure is converging numerically. At the point we stopped, we calculated the changes in the backscatter amplitudes and cross sections produced by $\tilde{J}$, $\tilde{L}$ and the altered L_{HR} and J_{VR}. We find

$$\begin{aligned} \delta\mathcal{B}_H(\hat{\kappa}) &= 4.7 \times 10^{-2} \exp(i\,72.7^\circ) \\ \delta\mathcal{B}_V(\hat{\kappa}) &= 1.6 \times 10^{-2} \exp(i\,168.3^\circ) \\ \delta\sigma_{HH} &= -7.7 \times 10^{-4} \text{ dB} \\ \delta\sigma_{VV} &= -4.4 \times 10^{-2} \text{ dB}. \end{aligned} \tag{40}$$

TABLE II
$\tilde{J}$ AND $\tilde{L}$ CONVERGENCE

Iteration Number	$\delta\tilde{J}$	$\delta\tilde{L}$
1	4.6×10^{-1}	8.7×10^{-3}
2	1.8×10^{-1}	7.2×10^{-5}
3	9.3×10^{-2}	6.9×10^{-7}
4	5.6×10^{-2}	Iteration stopped
5	3.7×10^{-2}	after $n = 3$ due to
6	2.6×10^{-2}	rapid convergence

These are very small changes and again emphasize the adequacy of the f_H and f_V assumption for the surface under consideration.

VI. Summary and Conclusions

The method previously developed for scattering from perfectly conducting azimuthally homogeneous surfaces has been successfully applied to scattering from azimuthally homogeneous surfaces that are imperfect conductors, where $\sqrt{\epsilon}$ has a large imaginary part. The extension involves solving simultaneously the top-side and the bottom-side integral equations by methods shown to have very low errors at X-band (10 GHz), even for such a highly curved surface as a sea wave in the deformation phase of breaking.

An example calculation at X-band demonstrates that the new method produces highly accurate amplitudes and cross sections for polarized backscatter from sea waves.[1]

Appendix
Computational Details

The wave form supplied by UCSB is a list of y, z values on a nonuniform path-length grid. For the surface used in this report, the path-length grid spacing varied from $\frac{1}{2}$ mm to 2.8 cm with the $\frac{1}{2}$ mm spacing used in the highly curved regions of the wave. To perform the underside integrals with the Hankel functions of complex argument, we require the surface to be sampled on a fine uniform path length grid. Here, we have used $\Delta\ell = \frac{1}{10}$ mm. The procedure used to define the surface at this scale is as follows. We first consider y and z as functions of the index (i). We then individually cubic spline interpolate y and z as functions of i. This yields continuous functions with continuous first and second derivatives. We then calculate the path length

$$\ell(i) = \int_0^i di' \left\{ \left(\frac{dy(i')}{di'} \right)^2 + \left[\frac{dz(i')}{di'} \right]^2 \right\}^{1/2} \tag{A.1}$$

determine the appropriate i for a given ℓ and calculate the six functions: $y(\ell)$, $y'(\ell)$, $y''(\ell)$, $z(\ell)$, $z'(\ell)$, $z''(\ell)$. The fine grid at 1/10 mm has 131 072 (2^{17}) points. The power of two is required because of the technique we use to solve (5) (see below). Most of this surface consists of flat regions both in front of and beyond the UCSB surface. The actual ℓ variable is taken to be zero near the center and corresponds to the peak of the UCSB surface. The variables ℓ_+ and ℓ_- are determined by adding 5 m of flat surface on either side of the UCSB surface so that $\ell_+ - \ell_- = 11.7$ m.

The reason we sample the surface at $\Delta\ell = \frac{1}{10}$ mm is that all integrals on the bottom side are calculated with this grid. Such a fine grid is required since $H_0^{(1)}(Z)$ and $H_1^{(1)}(Z)$ vary quite rapidly due to $\sqrt{\epsilon}$ having a large imaginary part. To further capture the rapid variations, we average $H_0^{(1)}(Z)$ and $H_1^{(1)}(Z)$ over a 1/10 mm interval when performing the bottom-side integrals.

Of course, we do not want to solve L_{HR} and J_{VR} on the fine grid since this would require an excessive number of calculations for an insignificant improvement in accuracy. Instead, we downsample by a factor of eight so that the grid for the top-side equations (28) and (29) is $\Delta\ell = 0.8$ mm; then there is a total of 14 623 grid points.

The numerical implementation of the stepping procedure has been discussed elsewhere [1] and will not be repeated here. We only note that we treat the $H_0^{(1)}$ singularity by averaging over the grid cell

$$H_0^{(1)}(0) \Rightarrow 1 + \frac{2i}{\pi}\left(\ell n \frac{\kappa \Delta\ell}{4} - 1 + \gamma_E \right) \tag{A.2}$$

where γ_E is Euler's constant

$$\gamma_E = 0.57721\cdots. \tag{A.3}$$

Finally, we turn to the solution of (5). We will here consider the H-pol equation, but the V-pol equation is solved in exactly the same manner. Since we know the solution for a flat plate, we define

$$J_{H0}(\ell) = \sqrt{\epsilon - \sin^2\theta}\, L_0 e^{-i\phi(\ell)} + \delta J(\ell) \tag{A.4}$$

so that the integral equation for δJ is

$$\tfrac{1}{2}\kappa \int_{-\infty}^{+\infty} d\ell' \delta J(\ell') H_0^{(1)}(Z) = L_0 X(\ell) \tag{A.5}$$

where

$$X(\ell) = e^{-i\phi(\ell)} + \frac{i}{2}\kappa \int_{-\infty}^{+\infty} d\ell' e^{-i\phi(\ell')} \cdot \left\{ \sqrt{\epsilon}\hat{n}(\ell') \cdot \hat{\gamma} H_1^{(1)}(Z) + i\sqrt{\epsilon - \sin^2\theta} H_0^{(1)}(Z) \right\}. \tag{A.6}$$

The function $X(\ell)$ is calculated on the 0.8-mm grid where for any ℓ we restrict the ℓ' integration in such a way that

$$|\ell' - \ell| \leq 3 \text{ cm}. \tag{A.7}$$

This is reasonable since

$$|H_0^{(1)}(Z)|_{\gamma=3\,\text{cm}} = 3.46 \times 10^{-8} \tag{A.8}$$

[1]For those readers wishing more detail in the derivation of the final equations, technical report LRDA-TR-2 190 003-002, June 1996, is available upon request from the authors.

for $\epsilon = 65 + i\,40$. Next, we rewrite (A.5) as

$$\begin{aligned}\tfrac{1}{2}\kappa \int d\ell'\, \delta J(\ell') H_0^{(1)}(\sqrt{\epsilon}\kappa|\ell' - \ell|) \\ = L_0 X(\ell) - \tfrac{1}{2}\kappa \int d\ell'\, \delta J(\ell')[H_0^{(1)}(\sqrt{\epsilon}\kappa\gamma) \\ - H_0^{(1)}(\sqrt{\epsilon}\,\kappa|\ell' - \ell|)]. \qquad \text{(A.9)}\end{aligned}$$

The left-hand side δJ can be solved for by FFT techniques if the right-hand side is known. Consequently, (A.9) is solved by iteration by first assuming $\delta J = 0$ on the right-hand side. Typically, four iterations are required to obtain a solution that changes less than 10^{-6} in δJ from its previously determined values. The iteration technique is particularly powerful here because of the short range of the kernel and the fact that over such short ranges $\gamma \sim |\ell' - \ell|$. Finally, we note that the right-hand side is calculated directly on the 0.8-mm grid and then interpolated to the $\frac{1}{10}$ mm grid by use of FFT's and zero padding.

REFERENCES

[1] D. Holliday, L. L. DeRaad, Jr., and G. J. St-Cyr, "Forward–backward: A new method for computing low-grazing angle scattering," *IEEE Trans. Antennas Propagat.*, vol. 44, pp. 722–729, May 1996.

[2] J. A. Saxton, "Electrical properties of water: Reflection characteristics of water surfaces at V.H.F.," *Wireless Engineer*, pp. 288–292, Sept. 1949.

[3] J. D. Jackson, *Classical Electrodynamics*, 2nd ed. New York: Wiley, 1975.

[4] W. T. Shaw and A. J. Dougan, "Half-space Green's functions and applications to scattering of electromagnetic waves from ocean-like surfaces," *Waves Random Media*, vol. 5, pp. 341–359, 1995.

[5] E. F. Knott, "Radar cross section," in *Radar Handbook*, M. I. Skolnik, Ed., 2nd ed. New York: McGraw-Hill, 1990, ch. 11.

[6] H. D. Ngo and C. L. Rino, "Application of beam simulation to scattering at low grazing angles: I Methodology and validation," *Radio Sci.*, vol. 29, pp. 1365–1379, 1994.

[7] P. Wang, Y. Yao, and M. P. Tulin, "An efficient numerical tank for nonlinear water waves, based on the multi-subdomain approach with BEM," *Int. J. Num. Meth. Fluids*, vol. 20, pp. 1315–1336, 1995.

[8] L. B. Wetzel, "Sea clutter," in *Radar Handbook*, M. I. Skolnik, Ed., 2nd ed. New York: McGraw-Hill, 1990, ch. 13.

Dennis Holliday received the B.S. degree in engineering science from Stanford University, Stanford, CA, in 1957, and the Ph.D. degree in theoretical physics from Princeton University, Princeton, NJ, in 1961.

In 1960 and 1961, he was a NATO Postdoctoral Fellow in theoretical physics. From 1963 to 1971 he was a Member of the Physics Department of the Rand Corporation, Santa Monica, CA, where he worked on scattering theory, quantum optics and quantum electronics, quantum statistical mechanics, nuclear proliferation technology, economics and policy, economics of nuclear power, and retirement plan formulation. He is currently with Logicon R&D Associates, Los Angeles, CA, where he conducts research for the Remote Imaging Program for the Office under the Secretary of Defense. His research interests include radar scattering theory, the generation and interaction of internal waves in the ocean, and remote sensing of the sea surface. He has published numerous reports and scientific papers.

Dr. Holliday is a member of the Working Group on Nuclear Proliferation and Arms Control of the California Arms Control and Foreign Policy Seminar, Phi Beta Kappa, Sigma Xi, and Tau Beta Pi.

Lester L. DeRaad, Jr. received the B.S. degree in physics from the University of Minnesota, Minneapolis, and the M.S. and Ph.D. degrees in physics from Harvard University, Cambridge, MA, in 1963, 1964, and 1970, respectively.

He served for several years as an Adjunct Assistant Professor at the University of California, Los Angeles, researching elementary particle physics; in particular, source theory, quantum electrodynamics, and strong and weak interaction phenomenology. He joined Logicon R&D Associates (LRDA), Los Angeles, CA, in 1978, where he participated in the SXTF/BACCARAT project for DNA, developing simple plasma models for colliding wires and accelerating foils in pulse power devices, and analyzing experimental data. He has conducted research in electromagnetic scattering, synthetic aperture radar, hydrodynamics, nuclear effects on communication systems, nuclear effects on radar systems, electromagnetic pulse, solid state physics, and plasma science. In 1987 he joined the Radar Ocean Imaging Project for the Office under the Secretary of Defense at LRDA, investigating electromagnetic scattering from random surfaces, studying hydrodynamic models of surface features of interest, and analyzing and interpreting experimental data.

Gaetan J. St-Cyr received the B.S., M.S., and Ph.D. degrees in electrical engineering from the California Institute of Technology, Pasadena, in 1962, 1963, and 1969, respectively.

He joined the Hughes Aircraft Company, Culver City, CA, where he participated in research optimization techniques for infrared scanning systems, atmospheric radiance and transmissivity, light scattering by atmospheric aerosols and clouds, IR background clutter, and missile countermeasure techniques. In 1971 he joined Cerberonics, Falls Church, VA, where he directed research in weapons systems analysis and the design of missile countermeasure devices. In 1975 he participated in the foundation of Poseidon research, where he managed programs on the recovery of sonar pulses buried in noise and on the detection of target signatures in random background noise. He created the Poseidon Hydro Code and numerical techniques to study fluid flow for hydrodynamic applications. In 1982 he joined Logicon R&D Associates, Los Angeles, CA, as a Research Scientist. He is presently working for the Office under the Secretary of Defense. His most recent research has been in the modeling of radar ocean imaging, signal detection, and data analysis.